Critical behavior and exchange splitting in the two-dimensional antiferromagnet Mn on Re(0001)

H. J. Elmers [1,*] Soumyajyoti Haldar [2] K. Medjanik,[1] S. Babenkov [1] O. Fedchenko,[1]
D. Vasilyev,[1] S. Heinze [2] and G. Schönhense[1]

[1]*Institut für Physik, Johannes Gutenberg-Universität, Staudingerweg 7, D-55099 Mainz, Germany*
[2]*Institute of Theoretical Physics and Astrophysics, University of Kiel, D-24098 Kiel, Germany*

We investigated the temperature-dependent electronic structure of the antiferromagnetic fcc-monolayer Mn on Re(0001) using vacuum-ultraviolet momentum microscopy. At $T = 25$ K the collinear, row-wise antiferromagnetic phase of the Mn monolayer results in a spin splitting of states. Density-functional theory, being in good agreement with the experimental results, reveals the spin and orbital projection of the observed electronic bands. The exchange split bands shift in opposite directions with increasing temperature, decreasing the exchange splitting of a pair of itinerant bands from 280 ± 10 meV at 25 K down to 185 ± 10 meV at the Néel temperature $T_N = 75 \pm 5$ K. The exchange splitting remains constant for $T > T_N$. The persisting exchange splitting is attributed to a remaining short-range, fluctuating antiferromagnetic order far above T_N.

I. INTRODUCTION

Antiferromagnets have attracted scientific interest as active materials in spintronics [1–3]. Thereby, the orientation of the sublattice magnetization acts as an information carrier, where the anomalous magnetoresistance effect enables readout. Electrical currents allow a manipulation, i.e., writing, of the sublattice magnetization as has been demonstrated for CuMnAs [4–6] and Mn_2Au [7–11] and attributed to the electronic structure [12].

The strong progress in active antiferromagnets also renewed the interest in the origin of magnetic order in antiferromagnets depending on dimensionality and localization of magnetic moments [13]. In the past, the effort to improve our understanding of finite-temperature magnetic order has mainly focused on ferromagnets. In the case of itinerant ferromagnets such as Fe, Co, and Ni, the temperature dependence of magnetic order has been explained by a one-electron finite-temperature band theory, known as Stoner theory [14,15]. The Stoner theory considers an exchange splitting Δ_{ex}, defined as the energetic difference between majority and minority spin bands. According to the Stoner theory, Δ_{ex} decreases with increasing temperature until it collapses at the Curie temperature simultaneously with long-range magnetic order. The Stoner theory simplifies the temperature dependence of electronic states to rigid band shifts of quasifree electrons, a condition that is obviously not fulfilled by the narrow energy d bands that are responsible for magnetism in real itinerant ferromagnets. Instead, strong correlation effects have to be considered, which are included in the framework of the local-band theory by local moments that remain constant but exhibit transverse fluctuations (Heisenberg model) [16]. Within the local-band theory, short-range spin order persists even above T_C although long-range spin order is lost at the ferromagnetic-paramagnetic phase transition [17]. Indeed,

transverse spin fluctuations have been observed on Ni(110) [18]. More recently, dynamical mean-field theory captures the persistent local magnetic moments above T_C in 3d ferromagnets using *ab initio* methods [19].

It is now widely accepted that the question whether or not the exchange splitting collapses in itinerant ferromagnets at or above T_C substantially depends on the degree of localization of the considered electron bands, which has to be compared with the size of regions that exhibit short-range spin order [20]. The analog basic information for antiferromagnets has not been directly addressed [21]. A collapse of the exchange splitting at the Néel temperature T_N has been measured for antiferromagnetic $MnBi_2Te_4$ [22,23]. Local moment lanthanide antiferromagnets show a residual splitting above T_N [24–26] and in the case of Tb for the $5d_z$-derived delocalized state, too [20].

Here, we focus on the itinerant two-dimensional antiferromagnet fcc-Mn/Re(0001), for which the collinear, row-wise antiferromagnetic order has been previously confirmed using low-temperature scanning tunneling microscopy [27]. The present paper reports the temperature-dependent exchange splitting in the antiferromagnetic monolayer Mn/Re(0001) across $T_N = 75$ K measured by momentum microscopy. Local density approximation theory reveals the spin and orbital character of the exchange-split bands in this system. The temperature-induced power-law reduction of the exchange splitting hints at a mixed behavior exhibiting characteristics of both the Stoner model and Heisenberg model. The persisting exchange splitting above T_N is a clear signature of a magnetic coherence length exceeding 3d band localization.

II. EXPERIMENTAL AND THEORETICAL METHODS

The Mn/Re(0001) samples have been prepared and investigated *in situ* in ultrahigh vacuum. We cleaned the Re(0001) surface by cycles of annealing in an oxygen atmosphere of 5×10^{-7} mbar at 1400 K and flashing at 1800 K followed
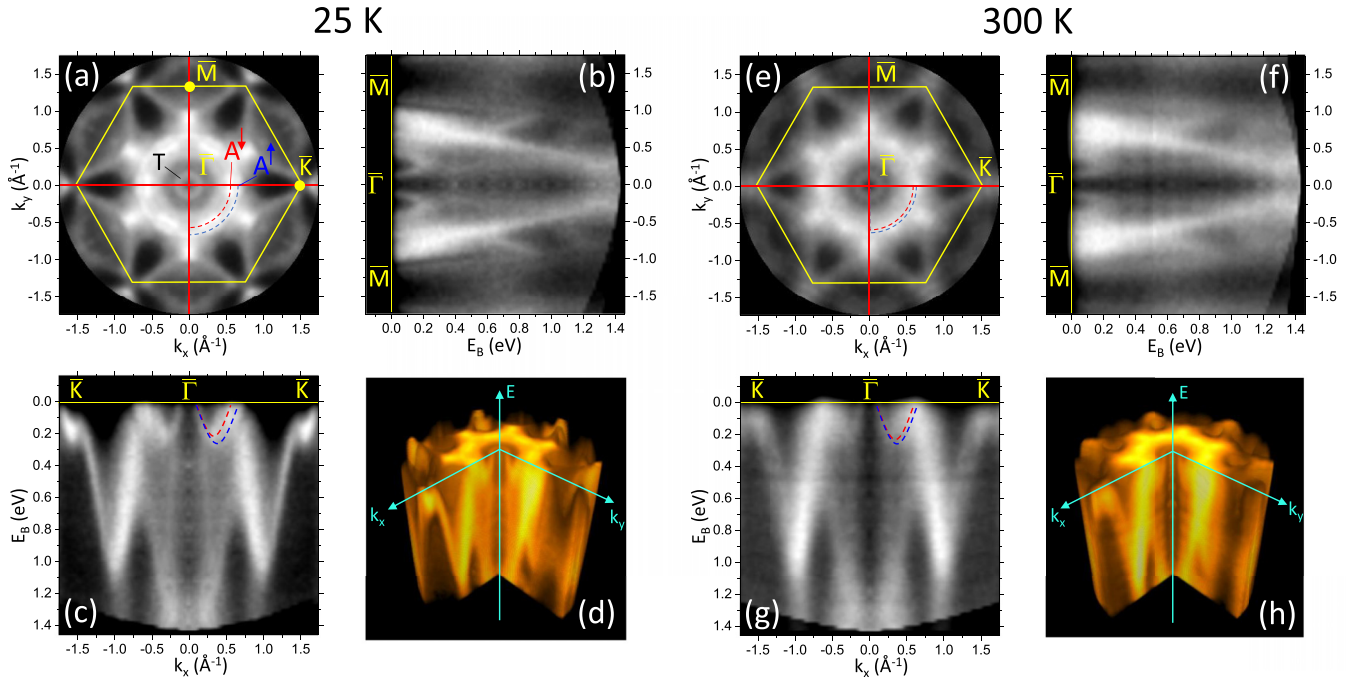
*elmers@uni-mainz.de

FIG. 1. Momentum microscopy of 1 ML Mn/Re(0001) ($h\nu = 21.2$ eV) for (a)–(d) $T = 25$ K and (e)–(h) $T = 300$ K. (a), (e) Constant energy maps $I(E_B, k_x, k_y)$ at $E_B = 60$ meV. (b), (f) Band dispersions $I(E_B, k_x = 0, k_y)$ shown as sections E_B vs k_y. (c), (g) Corresponding band dispersions along k_x. (d), (h) Cut three-dimensional representations of the $I(E_B, k_x, k_y)$ data array. [See magnified images (a) and (e) in the Supplemental Material [29]].

by a final flash at 1800 K as described in Ref. [28]. Ultrathin Mn layers have been grown by molecular beam epitaxy on the clean Re(0001) surface and annealed at 500 K. Mn grows on Re(0001) almost exclusively in fcc stacking [27]. The monolayer completion has been determined from the onset of Mn double layer states in the photoemission spectra (see Supplemental Material [29]).

For the photoemission experiments we used a single-hemisphere momentum microscope [30]. Photoelectrons were excited by He I light from a He discharge lamp ($h\nu = 21.2$ eV). The energy resolution has been set to 50 meV. The 3D $I(E_B, k_x, k_y)$ photoemission intensity arrays (E_B denotes the binding energy, and k_x and k_y the surface parallel momentum components) covering the full emission half space are recorded as a series of full-field images in energy steps with increments of 20 meV. To optimize the recorded intensity, we applied the large angular filling mode [30] resulting in a significant nonisochromaticity (α^2 term). The parabolic dependence on the k_y (dispersive) coordinate allows its numerical correction on the recorded data arrays. The probed sample area is about 0.03 mm^2. The intensity arrays for analyzing their temperature dependence were acquired for 90 s each during slowly cooling the sample.

Our theoretical calculations are based on density-functional theory (DFT) within the projector augmented-wave (PAW) [31] method as implemented in the VASP code [32,33]. We have performed spin-polarized calculations using Wigner-Seitz radii for the elements, i.e., $R_{\mathrm{Mn}}^{\mathrm{WS}} = 1.32$ Å for Mn and $R_{\mathrm{Re}}^{\mathrm{WS}} = 1.43$ Å for Re. As lattice parameters we used $a_{\mathrm{NN}} = 2.78$ Å , $c = 4.49$ Å, which were taken from Ref. [34] obtained via DFT within the generalized gradient approximation (GGA). Films with fcc stacking of the Mn monolayer were

structurally relaxed using the GGA exchange-correlation (xc) potential [35] in the row-wise antiferromagnetic state using a asymmetric film consisting of 20 Re(0001) layers with a Mn layer on top. The five uppermost layers were relaxed in the z direction, where the bulk reference is $c/2 = 2.24$ Å. We used $36 \times 20 \times 1k$ points in the irreducible wedge of the two-dimensional (2D) Brillouin zone (BZ) and a plane-wave basis set cutoff of $E_{\mathrm{max}} = 350$ eV. We have used a (2×1) supercell in order to design the row-wise antiferromagnetic state. We have used the VASPKIT [36] code to unfold the band structure that arises due to the use of the (2×1) supercell.

III. RESULTS

The experimental results shown in Fig. 1 reveal the difference of the band structure measured at 25 and 300 K. At 25 K, the constant energy map at the Fermi energy in Fig. 1(a), $I(E_F, k_x, k_y)$, shows the sixfold structure in reciprocal space resulting from an averaging over antiferromagnetic (AFM) domains with three possible directions of the sublattice magnetization. A double-circular pattern with a radius of 0.65 Å^{-1} is marked by the red dotted lines. The dispersion [Figs. 1(b) and 1(c)] of these states indicates an electronlike character with a velocity of 2 eV Å, being almost independent on the parallel momentum. The ring structure T in the center resembles the Tamm surface state of the bare Re(0001) surface but the diameter is considerably reduced (0.14 Å^{-1} compared to 0.3 Å^{-1} for clean Re) [37].

At 300 K, one observes changes in comparison to the data measured at 25 K. The splitting of the circular pattern decreases [Fig. 1(e)]. Yet, the dispersion of this split state
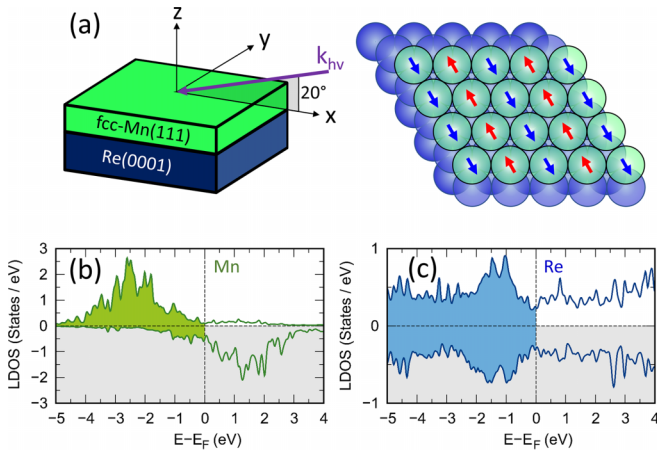
FIG. 2. (a) Sketch of the experimental geometry and the fcc-Mn(111)/hcp-Re(0001) monolayer with indicated row-wise antiferromagnetic structure. (b), (c) Local density of states (LDOS) for spin-up (positive) and spin-down (negative) states vs $E - E_F = -E_B$, orbital projected on a Mn sublattice atom (b) and neighboring Re atom (c).

appears similar as in the low-temperature state. In contrast, the smaller central ring has not changed at all.

Due to the Kramers degeneracy in antiferromagnets, spin-resolved momentum microscopy cannot identify the subband spin character for a specific sublattice. Instead, we performed *ab initio* calculations to reveal the spin character of the bands.

For the *ab initio* calculations we assumed the collinear row-wise antiferromagnetic magnetization structure of the fcc-Mn/Re(0001) monolayer in one out of three magnetic domains, as confirmed experimentally in Ref. [27] [see Fig. 2(a)]. Performing an orbital projection of the local density of states on one of the two magnetic Mn sublattices and neighboring Re atoms, we find local moments of $3.43 \mu_B$ for the Mn atom and $0.076 \mu_B$ for the neighboring Re atoms [see Figs. 2(b) and 2(c)]. The exchange splitting of localized Mn states amounts to ∼4 eV.

Figure 3 directly compares experimental low-temperature data and theoretical data along the high-symmetry direction $\overline{\Gamma}\text{-}\overline{K}$, which reveals the most prominent temperature-induced change of the band structure (see Supplemental Material [29] for the $\overline{\Gamma}\text{-}\overline{M}$ direction and alternative data representation). The color-coded calculated spectral weight nicely agrees with the experimentally observed photoemission intensity distributions. The overlaid spin character reveals a pair of exchange-split states crossing the Fermi level near $k_x = 0.6$ Å^{-1} with positive Fermi velocity. The marked pair, $A^{\uparrow}$ and $A^{\downarrow}$, relates to the split band pair discussed above (indicated as red dotted lines in Fig. 1). Both subbands merge into the band T that crosses E_F near $k_x = 0.15$ Å^{-1} with a negative Fermi velocity.

The remaining differences in the intensities of experimental and calculated bands are attributed to matrix-element-induced variations of the photoemission probabilities, which are not included in the calculations.

To quantify the temperature-induced changes of the electronic structure, we performed an analysis of intensity profiles
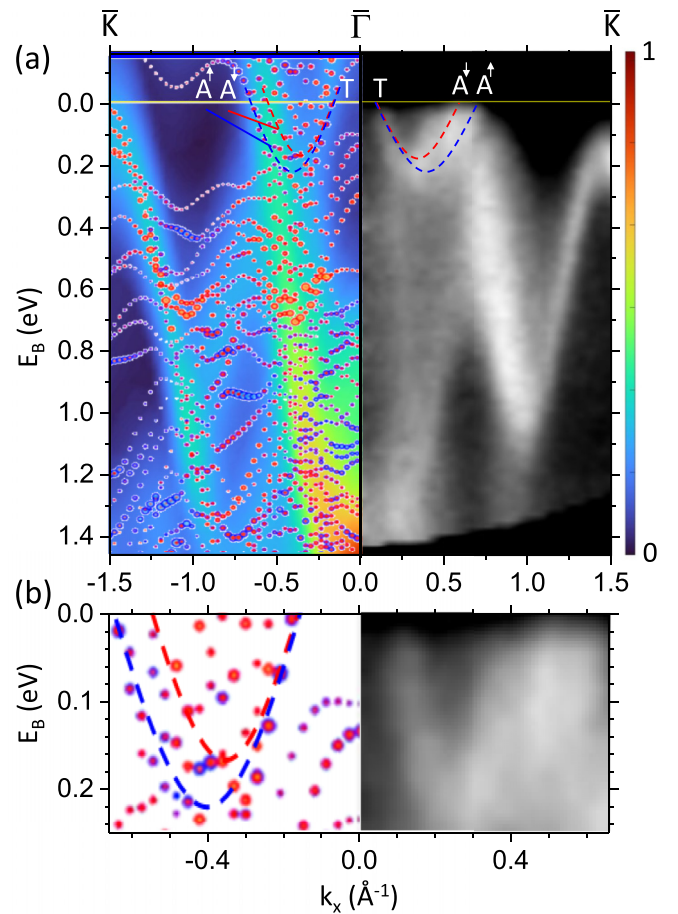

FIG. 3. (a) Comparison of experimental and theoretical data along the $\overline{\Gamma}\text{-}\overline{K}$ path. Left panel: Theoretical data in the k-resolved band density of states representation (color-coded intensity), overlaid by the density of summed orbitals located at the Mn atom, where the dot position indicates the eigenvalue and the dot size the spectral weight. The blue/red color indicates the two opposite spin states. Colored profiles and marks $A^{\uparrow}$, $A^{\downarrow}$ indicate the exchange-split band pair analyzed for their temperature dependence. Right panel: $I(E_B, k_x)$ map measured at 25 K and mirrored marks for the same pair of bands as for the theory data. (b) Magnified detail of (a). The blue/red dots denote the majority and minority band character, respectively, projected onto atomic orbitals. The size of the dots denotes the spectral weight of the projection.

across the split ring structure. The intensity maps depicted in Figs. 4(a)–4(c) have been measured for constant sample bias voltage set to a value that electrons excited at the Fermi energy at $k_y = 0$ are detected. Intensity profiles averaged over the indicated areas in Figs. 4(a)–4(c) are depicted in Fig. 4(d). The profiles are fitted with two Gaussian peak functions (accounting for profiles dominated by the experimental resolution) with fixed full width at half maximum of 0.12 Å^{-1} (solid lines) and a slowly varying function (dashed) to fit the background intensity. The five free parameters of the fit are the amplitude and the center of the two peaks and the amplitude of the background function. Restricting the fit to equal peak heights, as expected for exchange-split bands, has a minor influence on the peak positions. Similar fits were performed
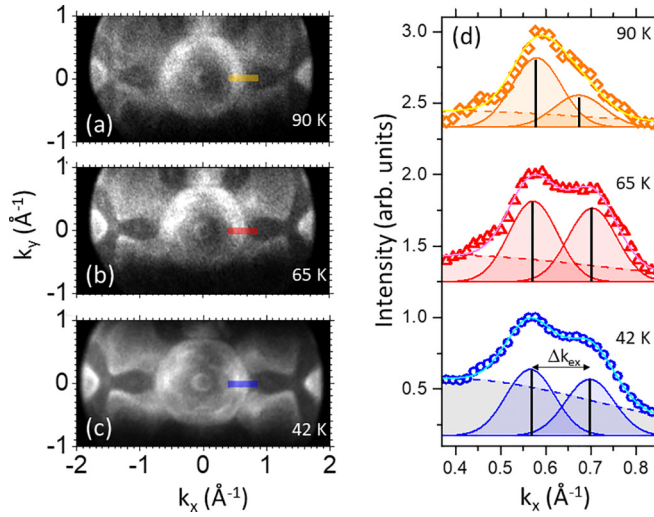
FIG. 4. (a)–(c) Selected $I(k_x, k_y)$ maps measured for constant sample voltage at the indicated temperatures. See Supplemental Material [29] for more profiles. The binding energy varies along k_y. (d) Intensity profiles along the lines indicated in (a)–(c). Solid lines correspond to fits with two Gaussian functions and a background function. Positions of the peak maxima are indicted.

for all data sets acquired during cooling (see Supplemental Material [29]).

The statistical noise results in the error bars as shown in Fig. 5. Besides the statistical error, systematic errors may originate from the varying background and local variations, which are most likely caused by an imperfect correction of the detector response function. These variations cause deviations of the fit curve from the data. The ratio of the intensity peaks of the exchange-split bands varies with temperature, which is unexpected. This is explained by an increase of the background function that in turn increases with decreasing temperature. The varying background may result from additional minority bands accompanying minority band A at
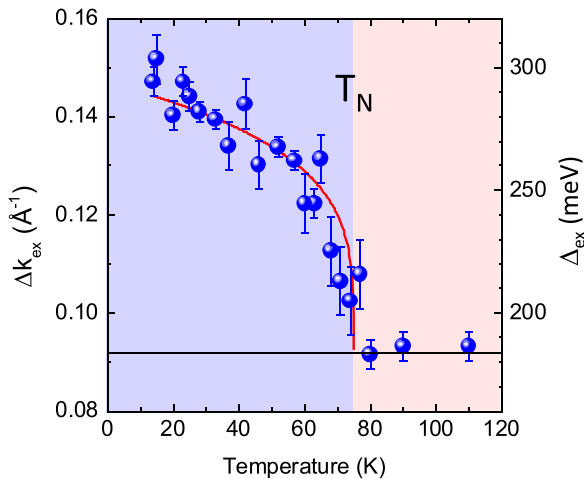

FIG. 5. Exchange splitting Δ_{ex} on the energy and Δk_{ex} on the momentum scale as a function of temperature. The solid line corresponds to a fit to the function $\Delta_{ex}(T) = \Delta_{ex}(T_N) + \Delta_{ex}(0)(1 - T/T_N)^\beta$ with the critical exponent $\beta = 0.5$.

smaller parallel momentum, which shift to larger momentum with increasing temperature due to the decrease of the exchange splitting and thus gradually shift into the fit window. An alternative explanation would be the adsorption of residual gases during the slow cooling process resulting in a nonstructured background with higher intensity near normal emission. The monotonous increase of the background with decreasing temperature rather points to surface contamination than to a result of the temperature-dependent exchange splitting, yet the statistical evidence is insignificant.

From the difference of the center positions, we determine the splitting value Δk_{ex} along the k_x axis. From the constant energy maps, one can deduce that Δk_{ex} is independent of the momentum direction. The exchange splitting on the energy scale results from $\Delta_{ex} = c_k \Delta k_{ex}$. Because c_k is independent on temperature, Δ_{ex} is proportional to Δk_{ex}.

The temperature dependence of Δ_{ex} (and Δk_{ex}) is depicted in Fig. 5. At the lowest temperature (14 K), we obtain $\Delta_{ex} = 300$ meV. Δ_{ex} continuously decreases with increasing temperature and assumes a value of 185 meV at 75 K. For higher temperatures, Δ_{ex} remains constant. A fit of this temperature dependence with the critical function $\Delta_{ex} - \text{const} \propto t^\beta$, with $t = T_N - T/T_N$ reveals the critical temperature for the antiferromagnetic phase transition, the Néel temperature $T_N = 75$ K. The critical exponent from the fit amounts to $\beta = 0.5^{+0.09}_{-0.11}$ (see Supplemental Material [29] for the determination of the critical exponent).

IV. DISCUSSION

It is useful to discuss the observed temperature dependence of the antiferromagnetic exchange splitting in view of previous results obtained for two-dimensional ferromagnets [38–40]. The observation that Δ_{ex} does not vanish at T_N but exhibits a constant value above T_N indicates a short-range antiferromagnetic order persisting up to at least 300 K. A similar behavior has been found for the rare earth ferromagnet Gd [20]. In contrast, the phase transition to a helical magnetic order results in a continuous reduction of Δ_{ex} [20,41,42]. Hence, we conclude that for Mn/Re(0001) the collinear antiferromagnetic state is stable even in the fluctuating phase above T_N. For the itinerant ferromagnet Ni, it has been observed that the exchange splitting decreased to zero by heating the sample above the Curie temperature [43]. Time-resolved photoemission experiments revealed a major influence of electron-magnon scattering for provoking this collapse [44]. Hence, the persistence of a significant exchange splitting well above T_N hints to an emerging collective behavior of valence electrons in Mn/Re(0001) beyond observations for itinerant ferromagnets [19,44–49] and even beyond local moment order in lanthanides [20,26] (see Supplemental Material [29] for details). Note that we observed a persistent exchange splitting for highly dispersive states in contrast to states at high-symmetry points with vanishing group velocities as in most previous studies. Thus, in comparison to ferromagnetism, antiferromagnetic order increases the magnetic moment localization behavior.

Alongside with the splitting, the critical exponent yields important information. In the case of leading ferromagnetic interaction, Monte Carlo simulations of the two-dimensional

Ising model results in $\beta = 1/8$, even if next-nearest-neighbor interactions are antiferromagnetic [50]. The theoretical value for the two-dimensional ferromagnetic XY model is $\beta \approx 1/4$ [51]. For leading antiferromagnetic order on a hexagonal lattice the critical behavior is more complex because of frustration. For a hexagonal lattice a simulated value of $\beta = 0.3$ has been reported [52,53]. All these models do not agree with the experimental value. The proposed mean-field universality class behavior [54] requires long-range exchange interactions. It is unlikely that these prevail in a Mn monolayer.

Finally, a renormalization-group study revealed that for the case of hexagonal symmetry chirality is a relevant operator associated with a new critical exponent [55]. In this case, one obtains $\beta = 0.5$ [52], in good agreement with our experimental result. A similar critical exponent has recently been measured in a three-dimensional layered system [10,22].

V. CONCLUSION

In conclusion, we have investigated the temperature-dependent surface electronic structure of the antiferromagnetic fcc-monolayer Mn on Re(0001) by means of momentum microscopy with 21.2 eV excitation. The prominent band (band *A*) is isotropic in (k_x, k_y) and shows an exchange splitting of 280 meV in the ground state that is reduced to 185 meV at $T > T_N = 75$ K. Low-temperature experimental data are in good agreement with density-functional theory. Theoretical results predict an exchange splitting of localized

Mn bands of ca. 4 eV. The exchange splitting of itinerant Mn bands is an order of magnitude smaller both in the low-temperature experiment and theory. The agreement of experiment and theory establishes the temperature-dependence of Δ_{ex} as a measure for the antiferromagnetic order parameter.

Temperature-dependent measurements reveal the variation of $\Delta_{ex}(T)$. In agreement with the Stoner theory, Δ_{ex} decreases when increasing T. In contrast to the Stoner theory Δ_{ex} remains finite and constant above T_N. This behavior can be understood from the short-range spin order persisting above the Néel temperature. The critical behavior of the temperature-dependent part of Δ_{ex} agrees better with renormalization-group theory using chirality as a relevant operator [55] than with a pure (Heisenberg-like) antiferromagnetic phase transition.

[1] T. Jungwirth, X. Marti, P. Wadley, and J. Wunderlich, Nat. Nanotechnol. **11**, 231 (2016).

[2] O. Gomonay, T. Jungwirth, and J. Sinova, Phys. Status Solidi RRL **11**, 1700022 (2017).

[3] V. Baltz, A. Manchon, M. Tsoi, T. Moriyama, T. Ono, and Y. Tserkovnyak, Rev. Mod. Phys. **90**, 015005 (2018).

[4] P. Wadley, B. Howells, J. Zelezny, C. Andrews, V. Hills, R. P. Campion, V. Novak, K. Olejnik, F. Maccherozzi, S. S. Dhesi, S. Y. Martin, T. Wagner, J. Wunderlich, F. Freimuth, Y. Mokrousov, J. Kunes, J. S. Chauhan, M. J. Grzybowski, A. W. Rushforth, K. W. Edmonds *et al.*, Science **351**, 587 (2016).

[5] M. J. Grzybowski, P. Wadley, K. W. Edmonds, R. Beardsley, V. Hills, R. P. Campion, B. L. Gallagher, J. S. Chauhan, V. Novak, T. Jungwirth, F. Maccherozzi, and S. S. Dhesi, Phys. Rev. Lett. **118**, 057701 (2017).

[6] P. Wadley, S. Reimers, M. J. Grzybowski, C. Andrews, M. Wang, J. S. Chauhan, B. L. Gallagher, R. P. Campion, K. W. Edmonds, S. S. Dhesi, F. Maccherozzi, V. Novak, J. Wunderlich, and T. Jungwirth, Nat. Nanotechnol. **13**, 362 (2018).

[7] S. Y. Bodnar, L. Smejkal, I. Turek, T. Jungwirth, O. Gomonay, J. Sinova, A. A. Sapozhnik, H. J. Elmers, M. Kläui, and M. Jourdan, Nat. Commun. **9**, 348 (2018).

[8] M. Meinert, D. Graulich, and T. Matalla-Wagner, Phys. Rev. Appl. **9**, 064040 (2018).

[9] M. Arana, M. Gamino, E. F. Silva, V. M. T. S. Barthem, D. Givord, A. Azevedo, and S. M. Rezende, Phys. Rev. B **98**, 144431 (2018).

[10] X. Chen, X. Zhou, R. Cheng, C. Song, J. Zhang, Y. Wu, Y. Ba, H. Li, Y. Sun, Y. You, Y. Zhao, and F. Pan, Nat. Mater. **18**, 931 (2019).

[11] S. Y. Bodnar, M. Filianina, S. P. Bommanaboyena, T. Forrest, F. Maccherozzi, A. A. Sapozhnik, Y. Skourski, M. Kläui, and M. Jourdan, Phys. Rev. B **99**, 140409(R) (2019).

[12] H. J. Elmers, S. V. Chernov, S. W. D'Souza, S. P. Bommanaboyena, S. Y. Bodnar, K. Medjanik, S. Babenkov, O. Fedchenko, D. Vasilyev, S. Y. Agustsson, C. Schlueter, A. Gloskovskii, Y. Matveyev, V. N. Strocov, Y. Skourski, L. Smejkal, J. Sinova, J. Minar, M. Klaeui, G. Schoenhense, and M. Jourdan, ACS Nano **14**, 17554 (2020).

[13] A. Barman, G. Gubbiotti, S. Ladak, A. O. Adeyeye, M. Krawczyk, J. Gräfe, C. Adelmann, S. Cotofana, A. Naeemi, V. I. Vasyuchka, B. Hillebrands, S. A. Nikitov, H. Yu, D. Grundler, A. V. Sadovnikov, A. A. Grachev, S. E. Sheshukova, J.-Y. Duquesne, M. Marangolo, G. Csaba *et al.*, J. Phys.: Condens. Matter **33**, 413001 (2021).

[14] E. Stoner, Proc. R. Soc. London, Ser. A **154**, 656 (1936).

[15] E. Wohlfarth, Rev. Mod. Phys. **25**, 211 (1953).

[16] V. Korenman, J. L. Murray, and R. E. Prange, Phys. Rev. B **16**, 4032 (1977).

[17] E. Weschke and G. Kaindl, J. Phys.: Condens. Matter **13**, 11133 (2001).

[18] A. Kakizaki, J. Fujii, K. Shimada, A. Kamata, K. Ono, K.-H. Park, T. Kinoshita, T. Ishii, and H. Fukutani, Phys. Rev. Lett. **72**, 2781 (1994).

[19] A. I. Lichtenstein, M. I. Katsnelson, and G. Kotliar, Phys. Rev. Lett. **87**, 067205 (2001).

[20] M. Bode, M. Getzlaff, A. Kubetzka, R. Pascal, O. Pietzsch, and R. Wiesendanger, Phys. Rev. Lett. **83**, 3017 (1999).

[21] A. Takayama, S. Souma, T. Sato, T. Arakane, and T. Takahashi, J. Phys. Soc. Jpn. **78**, 073702 (2009).

[22] D. A. Estyunin, I. I. Klimovskikh, A. M. Shikin, E. F. Schwier, M. M. Otrokov, A. Kimura, S. Kumar, S. O. Filnov, Z. S. Aliev, M. B. Babanly, and E. V. Chulkov, APL Mater. **8**, 021105 (2020).

[23] Y. J. Chen, L. X. Xu, J. H. Li, Y. W. Li, H. Y. Wang, C. F. Zhang, H. Li, Y. Wu, A. J. Liang, C. Chen, S. W. Jung, C. Cacho, Y. H. Mao, S. Liu, M. X. Wang, Y. F. Guo, Y. Xu, Z. K. Liu, L. X. Yang, and Y. L. Chen, Phys. Rev. X **9**, 041040 (2019).

[24] S.-E. Lee, Y. W. Windsor, A. Fedorov, K. Kliemt, C. Krellner, C. Schüßler-Langeheine, N. Pontius, M. Wolf, U. Atxitia, D. V. Vyalikh, and L. Rettig, Adv. Mater. Interfaces **9**, 2201340 (2022).

[25] M. Güttler, A. Generalov, M. M. Otrokov, K. Kummer, K. Kliemt, A. Fedorov, A. Chikina, S. Danzenbächer, S. Schulz, E. V. Chulkov, Y. M. Koroteev, N. Caroca-Canales, M. Shi, M. Radovic, C. Geibel, C. Laubschat, P. Dudin, T. K. Kim, M. Hoesch, C. Krellner, and D. V. Vyalikh, Sci. Rep. **6**, 24254 (2016).

[26] D. Wegner, A. Bauer, A. Rehbein, and G. Kaindl, Jap. J. Appl. Phys. **45**, 1941 (2006).

[27] J. Spethmann, S. Meyer, K. von Bergmann, R. Wiesendanger, S. Heinze, and A. Kubetzka, Phys. Rev. Lett. **124**, 227203 (2020).

[28] S. Ouazi, T. Pohlmann, A. Kubetzka, K. von Bergmann, and R. Wiesendanger, Surf. Sci. **630**, 280 (2014).

[29] See Supplemental Material at http://link.aps.org/supplemental/10.1103/PhysRevB.107.144424 for data similar to Fig. 3 but along $\overline{\Gamma}$-$\overline{M}$.

[30] G. Schönhense, S. Babenkov, D. Vasilyev, H.-J. Elmers, and K. Medjanik, Rev. Sci. Instrum. **91**, 123110 (2020).

[31] P. E. Blöchl, Phys. Rev. B **50**, 17953 (1994).

[32] G. Kresse and J. Furthmüller, Phys. Rev. B **54**, 11169 (1996).

[33] G. Kresse and D. Joubert, Phys. Rev. B **59**, 1758 (1999).

[34] D.-P. Ji, Q. Zhu, and S.-Q. Wang, Surf. Sci. **651**, 137 (2016).

[35] J. P. Perdew, K. Burke, and M. Ernzerhof, Phys. Rev. Lett. **77**, 3865 (1996).

[36] V. Wang, N. Xu, J.-C. Liu, G. Tang, and W.-T. Geng, Comput. Phys. Commun. **267**, 108033 (2021).

[37] H. J. Elmers, J. Regel, T. Mashoff, J. Braun, S. Babenkov, S. Chernov, O. Fedchenko, K. Medjanik, D. Vasilyev, J. Minar, H. Ebert, and G. Schönhense, Phys. Rev. Res. **2**, 013296 (2020).

[38] A. Bedoya-Pinto, J.-R. Ji, A. K. Pandeya, P. Gargiani, M. Valvidares, P. Sessi, J. M. Taylor, F. Radu, K. Chang, and S. S. P. Parkin, Science **374**, 616 (2021).

[39] D. L. Cortie, G. L. Causer, K. C. Rule, H. Fritzsche, W. Kreuzpaintner, and F. Klose, Adv. Funct. Mater. **30**, 1901414 (2019).

[40] U. B. Arnalds, J. Chico, H. Stopfel, V. Kapaklis, O. Bärenbold, M. A. Verschuuren, U. Wolff, V. Neu, A. Bergman, and B. Hjörvarsson, New J. Phys. **18**, 023008 (2016).

[41] B. Sinković, B. Hermsmeier, and C. S. Fadley, Phys. Rev. Lett. **55**, 1227 (1985).

[42] B. Hermsmeier, J. Osterwalder, D. J. Friedman, B. Sinkovic, T. Tran, and C. S. Fadley, Phys. Rev. B **42**, 11895 (1990).

[43] P. Poulopoulos, U. Bovensiepen, M. Farle, and K. Baberschke, J. Magn. Magn. Mater. **212**, 17 (2000).

[44] H.-S. Rhie, H. A. Dürr, and W. Eberhardt, Phys. Rev. Lett. **90**, 247201 (2003).

[45] C. J. Maetz, U. Gerhardt, E. Dietz, A. Ziegler, and R. J. Jelitto, Phys. Rev. Lett. **48**, 1686 (1982).

[46] H. Hopster, R. Raue, G. Güntherodt, E. Kisker, R. Clauberg, and M. Campagna, Phys. Rev. Lett. **51**, 829 (1983).

[47] M. Pickel, A. B. Schmidt, M. Weinelt, and M. Donath, Phys. Rev. Lett. **104**, 237204 (2010).

[48] S. Eich, M. Plötzing, M. Rollinger, S. Emmerich, R. Adam, C. Chen, H. C. Kapteyn, M. M. Murnane, L. Plucinski, D. Steil, B. Stadtmüller, M. Cinchetti, M. Aeschlimann, C. M. Schneider, and S. Mathias, Sci. Adv. **3**, e1602094 (2017).

[49] A. Hausoel, M. Karolak, E. Şaşıoğlu, A. Lichtenstein, K. Held, A. Katanin, A. Toschi, and G. Sangiovanni, Nat. Commun. **8**, 16062 (2017).

[50] B. Kutlu, Physica A **234**, 807 (1997).

[51] S. T. Bramwell and P. C. W. Holdsworth, Phys. Rev. B **49**, 8811 (1994).

[52] A. Mailhot, M. Plumer, and A. Caille, Phys. Rev. B **50**, 6854 (1994).

[53] H. Kawamura, J. Phys. Soc. Jpn. **61**, 1299 (1992).

[54] P. Azaria, B. Delamotte, and T. Jolicoeur, Phys. Rev. Lett. **64**, 3175 (1990).

[55] H. Kawamura, Phys. Rev. B **38**, 4916 (1988).